A Letters Journal Exploring the Frontiers of Physics

November 2016

EPL, **116** (2016) 49002
doi: 10.1209/0295-5075/116/49002

www.epljournal.org

Effect of the particle interactions on the structuration and mechanical strength of particulate materials

A. L. R. Sibrant[1,2] and L. Pauchard[1]

[1] *FAST, Univ Paris-Sud, CNRS UMR 7608 - F-91405, Orsay, France*
[2] *Department of Geological Sciences, University of Idaho - Moscow, ID, USA*

received 11 September 2016; accepted in final form 19 December 2016
published online 4 January 2017

PACS 91.60.Ba – Elasticity, fracture, and flow
PACS 83.80.Hj – Suspensions, dispersions, pastes, slurries, colloids
PACS 62.20.M- – Structural failure of materials

Abstract – We investigate the effect of the particles interaction on the mechanical strength of particulate materials. Starting from a dispersion of charged particles, the interparticle force can be modulated by the addition of ionic species. The structuration of the medium is then governed by the competition between drying and gelation processes. Rheological measurements show that addition of ionic species boosts the aggregation dynamics into a solid state and changes the structural properties of the final material. This last point is highlighted by precise measurements of i) the mechanical properties of particulate materials through crack pattern quantification, supported by indentation testing, and ii) the permeation properties during the drying process in a controlled geometry. In particular, these results show a decrease of the drained elastic modulus and an increase in the pore size when the ionic species content in the particulate material is increased. Hence, we show that the solid structure behaves mechanically as a network whose pore size increases when the electrostatic repulsion between particles is decreased. These results are consistent with the fact that the way particulate materials are structured determines their mechanical properties.

Introduction. – A way to form particulate materials is to dry a suspension of particles or to tune the physicochemical properties of a colloidal dispersion that passes to a gel phase. During the solidification, rheology can vary from viscous to elastoplastic properties, until the formation of brittle materials for dense colloidal systems. Many works make use of the wide range of mechanical properties of these systems and of the possibility to tune their mechanical behaviors [1–3]. Moreover, understanding the relation between macroscopic behavior and structural properties is of great interest in many industrial applications including coatings, ceramics or food science dealing with particulate materials. In particular, benefits are large multi-scale utilities in analogue modeling, especially to understand the dynamic of Earth processes [4–6]. Depending on their structures, solid materials can respond to a stress through mechanical instability: as an example, the occurrence of cracking can be more or less delayed as a result of a mismatch between the solid strength and the stress buildup (see illustration in fig. 1).

The macroscopic behavior depends on the size, shape, polydispersity, and concentration of the particles, the mechanical properties of the particles themselves and the interparticle forces. In the present work we investigate solidification of dispersions of charged colloids, tuning the interparticle forces through addition of ionic species to the dispersion [7,8]; the resulting electrostatic repulsion between colloids is thus decreased allowing the attractive van der Waals forces (which are essentially unaffected by salt) to play a more important role. First gelation kinetics are performed through rheological measurements and show a strong dependence with the quantity of ionic species added to the dispersion. This strong dependence also applies in the solid phase when quantifying i) the mechanical properties through the response of the material to drying stress, and ii) the permeation properties through drying kinetics. These experimental results are consistent with a scaling law that relies on elastic properties of the particulate material to the pore size. We show that the solid structure behaves mechanically as a network whose pore size

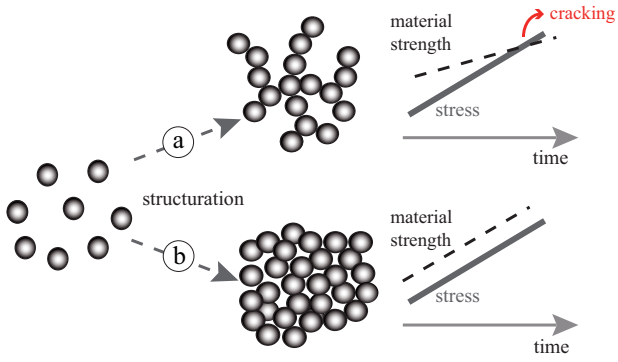

Fig. 1: (Colour online) The mechanical response of a particulate material to a stress depends on its microstructure. The strength of a particulate material is affected by the structuration, *e.g.*, gelation or fractal aggregation, resulting in different compactness. During a stress build-up, (a) materials with a low strength exhibit only low resistance to the stress, consequently mechanical instabilities, such as crack, release the stress, or (b) materials with a high strength can resist the stress.

increases when the electrostatic repulsion between particles is drecreased. These results are consistent with the fact that enhancement of the attractive force between particles build bigger, and mechanically weaker, structures.

Materials and methods. – The experiments were carried out at the FAST laboratory on a typical silica sol (Ludox HS40) exhibiting well-controlled physicochemical properties. The mean particle radius is $a = 7\,\mathrm{nm}$, and the solid volume fraction is 0.24 from measurements by dry extract at 150 °C. At a *p*H of 9.2 the particle surface bears a high negative charge density. In the absence of evaporation, the colloidal dispersion is stable due to the competition between van der Waals attraction and electrostatic repulsion [9]. However, the addition of ionic species to the colloidal dispersion may screen out the electrostatic interactions; consequently, the potential barrier decreases (fig. 2(a)). When the particles overcome the repulsive barrier, gelation of the dispersion may occur. In the present work, a solution of NaCl in water is added to the colloidal dispersion; the particle volume fraction of the resulting solution is $\phi_0 = 0.22$. The total salt concentration of the solution, *e.g.*, the ionic strength I since NaCl is monovalent, is adjusted up to $0.3\,\mathrm{mol}\cdot\mathrm{l}^{-1}$; note that the salt content of the initial suspension was estimated to $0.03\pm0.02\,\mathrm{mol}\cdot\mathrm{l}^{-1}$ using electrical conductivity. This is lower than the critical coagulation concentration, *ccc*, above which interfacial particle saturation can take place (the *ccc* is estimated at $0.46\,\mathrm{mol}\cdot\mathrm{l}^{-1}$ taking into account the measurements of the zeta potential of the particles ($-32\,\mathrm{mV}$ at *p*H 9.0) of our solutions in accordance with ref. [8][1]). The gelation kinetics was investigated through rheological measurements using an imposed shear rate rheometer (Contraves LS30)

[1]Changing the units, the *ccc* can be expressed as $0.8\,\mathrm{mg/m^2}$; this can be compared to the concentration of adsorbed amount saturating particles at $1\,\mathrm{mg/m^2}$ [10].

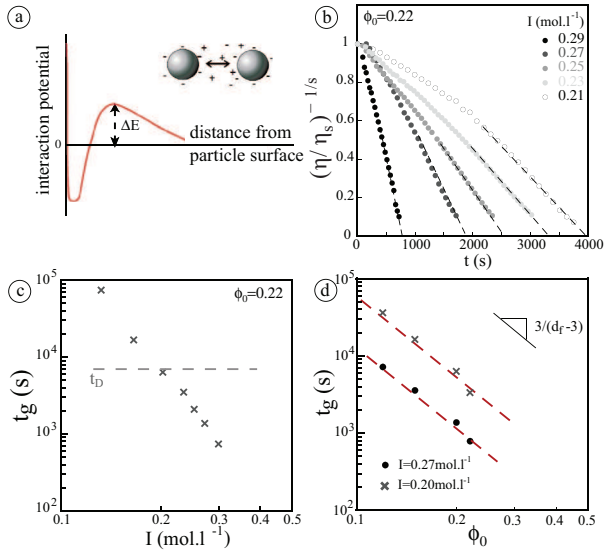

Fig. 2: (Colour online) (a) Repulsive barrier ΔE in a dispersion of charged particles. (b) Dimensionless viscosity, $(\eta/\eta_s)^{-1/s}$, *vs.* time of HS40 silica dispersion for different ionic strengths I: the exponent s is chosen to fit the measurements along a straight line when $t \to t_g$ ($s = 1.7$). (c) Resulting gelation time, t_g, *vs.* ionic strength I for a given particle volume fraction $\phi_0 = 0.22$ in log-log scale. (d) Gelation time, t_g, *vs.* initial particle volume fraction, ϕ_0, for two different ionic strengths $I = 0.20\,\mathrm{mol}\cdot\mathrm{l}^{-1}$ and $I = 0.27\,\mathrm{mol}\cdot\mathrm{l}^{-1}$ in log-log scale; the dashed lines determine the fractal dimension d_f of the clusters.

as shown in fig. 2(b). In the absence of evaporation, the viscosity η of salted dispersions increases first slowly, then sharply, and finally diverges [7]. This time variation can be interpreted by a percolation model of gelation transition allowing us to define the gelation time, t_g: $\eta \sim \eta_s/(t-t_g)^s$, where η_s is the viscosity of the solvent [1]. This behaviour is captured in the time variation of the dimensionless quantity $(\eta/\eta_s)^{-1/s}$ in fig. 2(b). The resulting variation of t_g with the ionic strength is shown in fig. 2(c). The variation of t_g as a function the particle volume fraction, keeping I constant, is obtained after dilution of the silica dispersion using pure water (MilliQ quality, resistivity: $18\,\mathrm{M\Omega}\cdot\mathrm{cm}$) by addition of NaOH to maintain a constant $p\mathrm{H} = 9.2$ (fig. 2(d)).

The mechanical properties of the solid structures are measured using two methods. i) The first method is based on the quantification of the crack morphologies induced by the drying process (fig. 3(a)). Indeed, the crack spacing reflects some mechanical properties of the fractured material, particularly the elastic modulus, E_p. In this way, a quantity of the colloidal dispersion mixed with a controlled salt content is deposited in a circular glass Petri dish (inner diameter $\sim 5.6\,\mathrm{cm}$). The solution is left to dry from the free surface, the evaporation being limited by diffusion of water into the air (at temperature, 22 °C, and relative humidity, $RH = 50\%$). The Petri dish is placed on a scale (Sartorius) allowing us to measure accurately the variation of the mass during the drying. A ring, 1 cm

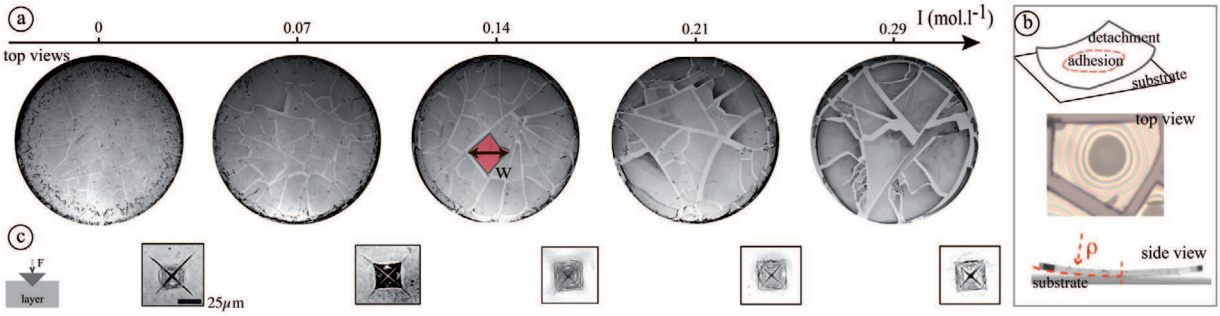

Fig. 3: (Colour online) (a) Crack patterns at the final stage of the drying process for particulate layers exhibiting different ionic strengths, I. (b) Partial delamination of a fragment at the final stage of the drying. Top view: interference fringes reveal the curvature of the transparent layer; side view of the curled fragment. (c) Optical micrographs of indentation prints in fragments of corresponding salted layers, using a pyramidal tip (maximum applied force $F = 100\,\mathrm{mN}$).

wide), covers the upper edge of the circular dish to saturate the air in water vapor and so to limit the evaporation effect at the border (see sketch in fig. 4(b)). When the solid phase is formed, the layer exhibits an approximately constant thickness, $h = 300 \pm 5\,\mu\mathrm{m}$, in the central region. The drying timescale t_d is defined as $t_d = h/V_E$, where V_E is the evaporation rate. Cracks formation is recorded using an interval timer with a camera positioned on the top of the sample. ii) The second method uses indentation testing to measure the mechanical response of the material to external force using a spherical tip as an indenter of radius $R = 0.25\,\mathrm{mm}$ assumed to be perfectly rigid (CSM Instruments Micro Indentation Tester, MHT). Measurements are performed on the same layers as in i), at time $t_c + \Delta t$; Δt is chosen such as $t_c + \Delta t$ has the same value for each system. Starting with the indenter in contact with the surface of the solid film adhering to a rigid substrate, the tip is driven inside the sample with a fixe loading speed $100\,\mathrm{mN/min}$. The applied force F is then measured as a function of the penetration depth p as shown in fig. 4(a)[2]. Assuming the material purely elastic within the limits of small deformation, the elastic response is well fitted by the Hertz contact law over a range of indentation depths as shown in the load-displacement curve in fig. 4(a). Thus, accordingly with the classical Hertzian model, the applied indentation force F is determined by [11] $F = \frac{4\sqrt{R}}{3(1-\nu^2)} E_p p^{3/2}$, ν being the Poisson ratio of the material (we use the value $\nu = 0.3$).

The permeation properties of particulate materials have been investigated through drying kinetics measurements. Indeed, the mass variation with time allows us to measure precisely the diffusivity of the porous material provided a well-defined geometry. The drying geometry used is a glass capillary tube exhibiting a single circular surface of evaporation (diameter $\sim 2\,\mathrm{mm}$), while the top of the tube is closed (fig. 5(a)). The inner wall of the capillary tube is hydrophobized to reduce adhesion of the solid and consequently to avoid the formation of cracks contrary to previous works [4]. The vertical tube is partially filled with a controlled mixture of the colloidal dispersion and the salted water, and is placed on a scale. The mass variation of the wet gel with time is measured during the evapora-

[2]Note that this method does not intend to give absolute quantities but it provides a robust procedure to compare mechanical properties of different materials.

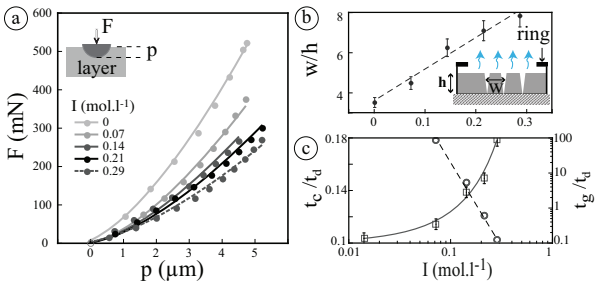

Fig. 4: (Colour online) Mechanical properties of salted colloidal layers. (a) Spherical indentation load-displacement (applied force F *vs.* penetration depth p) for particulate layers exhibiting different ionic strengths, I (lines are Hertz contact theory). (b) Dimensionless variation of the crack spacing w/h *vs.* ionic strength I (the dashed line is a guide for the eye). (c) Dimensionless delay in cracking, t_c/t_d (semi-log scale), and dimensionless gelation time, t_g/t_d, (log-log scale) as a function of the salt content; the plain line is a theoretical model.

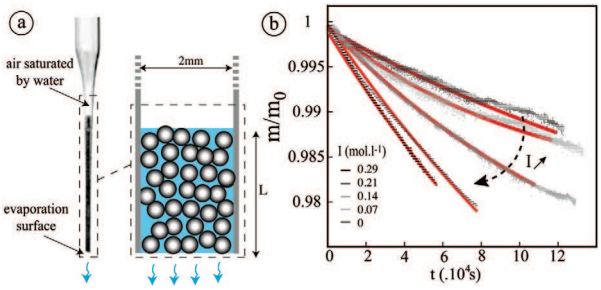

Fig. 5: (Colour online) Permeation properties of gelled layers. (a) Setup: drying process from capillary tube. (b) Time variations of the mass during the drying of gels having different salt contents, I; measurements are grey dots and curve-fitting is shown by plain lines.

tion process (at temperature, 22 °C, and relative humidity, $RH = 50\%$). Results are fitted by the stretched exponential function: $\frac{m(t)-m_\infty}{m_0-m_\infty} = \exp[-(\frac{\chi_1^2 D_p t}{L^2})^{\chi_2}]$, where m_0 and m_∞ are reference values, and D_p is the effective poroelastic diffusivity of the different porous materials ($\chi_1 \sim 2.4$, $\chi_2 \sim 1$) [12,13].

Results and discussion. – We assume a homogeneous diffusion of salt in the layer, leading to a possible deposit of salt around the contacts between particles at high salt concentration. At very high concentration of salt ($I > 1\,\mathrm{mol \cdot l^{-1}}$), measurements of the elastic modulus reveal a mean value that does not depend on the ionic strength anymore (taking into account the large uncertainty of the measurements, $\sim 15\%$). The mean value is lower than the values obtained for ionic strength up to $0.3\,\mathrm{mol \cdot l^{-1}}$ (for $I > 1\,\mathrm{mol \cdot l^{-1}}$, we found $E_p/E_p^0 = 0.2$). In view of these observations the measurements of mechanical properties at high ionic strength ($I > 1\,\mathrm{mol \cdot l^{-1}}$) seem to be strongly affected by the presence of salt, while, up to $0.3\,\mathrm{mol \cdot l^{-1}}$ the continuous variation of the physical parameters as a function of the salt content seem to reflect the microstructure of the salted colloidal materials.

The solidification of a colloidal dispersion induced by evaporation of the solvent strongly depends on the suspension salt content. In this way, the structuration is governed by the competition between drying and gelation processes. We characterize these processes by two timescales: i) the drying time, t_d, that is related to the loss of free volume, and ii) the gelation time, t_g, that exhibits a strong power law dependence with the ionic strength as shown in fig. 2(d). Physically, the timescale t_g is the duration elapsed between the sample preparation and the gelation transition. Thus, at time t_g an aggregate is expected to connect all the volume of the system. In the following, the timescale t_d is kept constant under fixed relative humidity and temperature. At low ionic strengths, $t_d < t_g$, solidification is governed by the solvent removal. However, at large ionic strengths, $t_g < t_d$, the appearance of an elastic behaviour is mainly induced by the gelation process and the kinetics of the structuration is even more rapid if the salt content is high. When the interaction between particles is strongly attractive, the formation of fractal aggregates is more favorable. The gelation time is predicted to vary as a function of the volume fraction of particles ϕ_0 with an exponent that is related to the fractal dimension of the clusters, d_f [8]: $t_g \propto \phi_0^{3/(d_f-3)}$ [14]. Rheological measurements lead to $d_f = 2.1$ for $I = 0.27\,\mathrm{mol \cdot l^{-1}}$ suggesting compact clusters in accordance with previous studies [1] (fig. 2(d)). Moreover, measurements do not show significant variations of the fractal dimension changing the ionic strength from $0.20\,\mathrm{mol \cdot l^{-1}}$ to $0.27\,\mathrm{mol \cdot l^{-1}}$ (fig. 2(d)).

Depending on the structuration of the colloidal dispersion, the mechanical properties of the solid network will be significantly modified. One direct effect of the presence of salt content on the mechanical properties of the

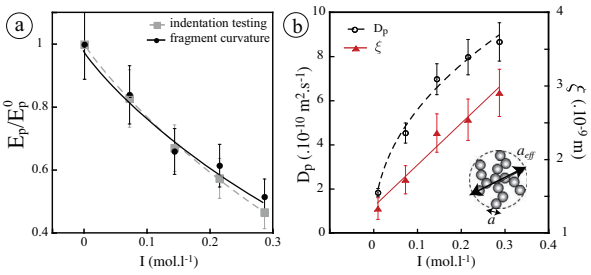

Fig. 6: (Colour online) (a) Influence of the ionic strength on the drained elastic modulus E_p (E_p^o is the property value without salt addition); measurements result from indentation testing and crack pattern quantification. (b) Influence of the ionic strength on the poroelastic diffusivity, D_p, and the pore size, ξ, of the solid gel.

structure is illustrated in fig. 3(a). Upon evaporation, drying stress build-up induces shrinkage of the network that is frustrated by adhesion on the substrate. This differential expansion results in the formation of a polygonal crack pattern. Classically, the way the material withstands the stress, leading to more or less cracking, will reflect the mechanical strength of the materials. The key parameter to characterize a network of cracks is the crack spacing, *e.g.*, fragment size, that usually scales with the layer thickness. Here, under constant drying conditions, the mean crack spacing, w, increases with the ionic strength as shown in fig. 4(b). This variation reflects a variation of the mechanical properties with the ionic strength since only a slight increase of the layer thickness, $\sim 5\%$, takes place with increasing the salt content. Moreover, for such thick layers, further stress release leads to a delamination process [15] (fig. 3(b)). Measurements of the curvature, ρ^{-1}, of the warped layer allow us to determine the relevant elastic modulus, E_p as $\rho \sim \frac{E_p h^3}{12M}$, where M is the moment per unit depth estimated by $M \sim (-P_{cap})h^2$ with P_{cap} the capillary pore pressure [16,17]. The mean curvature of fragments is found to increase with the ionic strength. As a result, the elastic modulus of the solid decreases with the presence of salt (fig. 6(a)). These results are supported by analysis using indentation testing (fig. 4(a)); these last measurements are operated 30 minutes late after the final crack formation, and allow us to extract the elastic modulus using the Hertz contact law (fig. 6(a)).

The decrease of the mechanical strength with the presence of salt suggests a higher capability to deform elastically under the effect of a stress before cracking. This consideration is emphasized since the presence of salt postpones the occurrence of cracking under fixed drying conditions (fig. 4(c)). The period of time elapsed between the layer deposition and the moment of the first crack to appear is denoted by t_c. Measurements show a clear increase of t_c with the ionic strength (fig. 4(c)). At first sight, this is a striking result, particularly when $t_g/t_d > 1$ since the solid structure is formed more rapidly through gelation process. We then expect a response to external

stress, here the capillary stress induced by evaporation, more rapid through the formation of cracks. Simple considerations on poroelasticity show that the elapsed time for cracking increases when the mechanical strength of the material weakens as $\frac{t_c}{t_d} = \frac{-P_{cap}}{E_p}$ [17]. This equation together with the measurements of E_p from fig. 6(a) well fit the experimental date as shown in fig. 4(c).

The significant delay before cracking is highlighted by the following considerations using indentation testing. Here a four-sided pyramidal tip (Vickers) is used to obtain qualitative information on the cohesion of the material. Indeed, optical micrographs of indentation prints performed at a maximum force 100 mN show radial cracks from the indent (fig. 3(c)). The mean length of the radial cracks gives a way to estimate the brittleness of a material. This is captured through the fracture toughness, K_c, that represents the material resistance to fracture[3]. Classically, the fracture toughness is related to the elastic modulus of the material and to the fracture surface energy Γ by $2\Gamma = K_c^2(1-\nu^2)/E_p$. The mean length of the radial cracks from the indent decreases with the presence of salt suggesting a less brittle material with increasing salt content. Consequently, this suggests an increasing trend of the fracture toughness, K_c, with increasing salt content. Note that experimental results do not indicate any plastic behaviour of the materials; however this does not exclude the effect of the salt content on the plastic behaviour. From the variations of both E_p and K_c with the presence of salt, the fracture surface energy, Γ, is expected to increase with the salt content. This statement is consistent with the fact that the increase of the ionic strength is in favor of the attractive interactions between particles.

The modification of structure induced by the addition of salt is also associated with the change in permeation properties of the system. The consolidation of a particulate material is related to a slow flow of the liquid through the solid network. A key parameter to characterize this flow is the poroelastic diffusivity D_p of the gel given by $D_p = E_p k/\eta_s$, where k is the permeability depending on the pore size as ξ as $k \sim \xi^2$. Precise measurements of the drying kinetics in the geometry of a capillary tube allow us to determine the poroelastic diffusivity (fig. 5(a)). At high ionic strength ($0.2\,\mathrm{mol}\cdot\mathrm{l}^{-1} < I$), the bulk of the solution rapidly forms a solid phase on a height L from the surface of evaporation. However, at low ionic strength ($I < 0.2\,\mathrm{mol}\cdot\mathrm{l}^{-1}$), advection of particles induced by the evaporation overcomes the gelation process. The wet structure grows from the evaporation surface. Once the height of the wet structure reaches the value L, the upper liquid solution is removed; further growth of the structure is then stopped, and this allows us to compare the drying kinetics of wet structures in the same geometry.

[3]These considerations are only qualitative and do not allow us to extract the fracture toughness of the material since the length of radial cracks are not longer than 2 times the print diameter [18].

The diffusivity D_p is estimated from curve-fitting the experimental data as shown in fig. 5(b). The influence of the ionic strength on the diffusivity, and on the pore size variation, is shown in fig. 6(b). Consequently, the following scaling law is derived from experimental data:

$$\xi \sim a_0 + \alpha I^{\beta} \tag{1}$$

with $\beta \sim 1$. a_0 corresponds to the pore size without salt addition. Such a dependence has been obtained on agarose solutions through AFM images [19].

In the following, we rely on this I-dependence of the pore size and the elastic properties of the medium. Light-scattering studies of colloidal silica gels have shown a power law concentration dependence for the characteristic cluster dimension, a_{eff} (sketch in fig. 6(b)) [20,21]. In this way, at gelation, we identify an effective particle volume fraction of the clusters, ϕ_{eff}, such as

$$\frac{a_{eff}}{a} \sim \left(\frac{\phi_{eff}}{\phi}\right)^{\frac{1}{3-d_f}}, \tag{2}$$

where ϕ is the particle volume of the individual colloidal particles. Assuming the pore size scales with the characteristic cluster dimension, it becomes

$$\xi \sim (1-\phi_{eff})^{\frac{1}{3-d_f}}. \tag{3}$$

Furthermore, a model well established shows that the elastic modulus of a particle assembly should vary as the fourth power of the particle packing fraction [22]:

$$E_p \propto \phi^4. \tag{4}$$

Incorporating the effective particle volume fraction, ϕ_{eff}, from eq. (3), and combining with eq. (4) lead to the following equation for the elastic modulus:

$$E_p \propto [1 - b\xi^{3-d_f}]^4. \tag{5}$$

Capturing the fractal dimension from rheological measurements (fig. 2(d)), eq. (5) together with the scaling law (1) well describe the variation of the elastic modulus as a function of the ionic strength as shown in fig. 6. Therefore, the solid structure behaves mechanically as a network whose pore size increases with the ionic strength, also exhibiting a less dense network of solid particles.

Conclusion. – We have shown that the nature of interactions between charged particles in a dispersion strongly influences its structuration and the mechanical properties of the final particulate material. Indeed, rheological measurements show that decreasing the electrostatic repulsion between particles, through the increase of the salinity, boosts the aggregation dynamics into a solid state and changes the structural properties of the final material. The last point is highlighted by the direct observation of cracking upon drying: increasing the salinity reveals an increase of the time-lag breaking, and the crack spacing

and/or curling surface reflects a decrease of the mechanical strength of the material. These results are consistent with a less dense structure, exhibiting an increase of its pore size with the salinity. This has been demonstrated through measurements of the permeation properties during the drying process in a controlled geometry. The results allow us to determine scaling laws that relate elastic properties of material to pore size, in accordance with existing predictions.

* * *

We would like to thank Bernard Cabane, Anne Davaille, and Eric Mittelstaedt for valuable discussions, and Alban Aubertin, Lionel Auffray, and Rafael Pidoux for engineering and technical support.

REFERENCES

[1] Brinker C. J. and Scherer G. W., in *Sol-Gel Science: the Physics and Chemistry of Sol Gel Processing* (Academic, San Diego) 1990.
[2] Boulogne F., Pauchard L., Giorgiutti-Dauphiné F., Botet R., Schweins R., Sztucki M., Li J., Cabane B. and Goehring L., *EPL*, **105** (2014) 38005.
[3] Kitsunezaki S., Nakahara A. and Matsuo Y., *EPL*, **114** (2016) 64002.
[4] Gauthier G., Lazarus V. and Pauchard L., *EPL*, **89** (2010) 26002.
[5] Di Giuseppe E., Davaille A., Mittelstaedt E. and Francois M., *Rheol. Acta*, **51** (2012) 451.
[6] Di Giuseppe E. and Davaille A., *Geophys. Res. Abstr.*, **23** (2010) 07954.
[7] Pauchard L. and Allain C., *Phys. Rev. E*, **59** (1999) 3737.
[8] Trompette J. L. and Meireles M., *J. Colloid Interface Sci.*, **263** (2003) 522.
[9] Iller R. K., *The Chemistry of Silica* (Wiley Interscience) 1979.
[10] Wong K. *et al.*, *J. Colloid Interface Sci.*, **153** (1992) 55.
[11] Johnson K. L., *Contact Mechanics* (Cambridge University Press, London) 1985.
[12] Crank J., *The Mathematics of Diffusion*, Vol. **9** (Clarendon Press, London, UK) 1975, p. 30.
[13] Chung J. Y., Regev I. and Mahadevan L., *Soft Matter*, **12** (2016) 7855.
[14] Allain C., Cloitre M. and Wafra M., *Phys. Rev. Lett.*, **74** (1995) 1478.
[15] Pauchard L., *Europhys. Lett.*, **74** (2006) 188.
[16] Landau L. and Lifshitz E. M., *Theory of Elasticity*, 3rd edition (Pergamon Press, New York) 1986.
[17] Giorgiutti-Dauphiné F. and Pauchard L., *Eur. Phys. J. E*, **37** (2014) 39.
[18] Malzbender J., den Toonder J. M. J., Balkenende A. R. and de With G., *Mater. Sci. Eng. R*, **36** (2002) 47.
[19] Ioannidis N., Bowen J., Pacek A. and Zhang Z., *J. Colloid Interface Sci.*, **367** (2012) 153.
[20] Cabane B., Dubois M., Lefaucheux F. and Robert M. C., *J. Non-Cryst. Solids*, **119** (1990) 121.
[21] Dietler G., Aubert C., Cannell D. S. and Wiltzius P., *Phys. Rev. Lett.*, **57** (1986) 3117.
[22] Kendall Z., Alford N. and Birchall J. D., *Proc. R. Soc. Lond. A*, **412** (1987) 269.